Available online at www.sciencedirect.com
SCIENCE DIRECT®
Journal of Magnetic Resonance 163 (2003) 139–148
JMR Journal of Magnetic Resonance
www.elsevier.com/locate/jmr

Processing DOSY spectra using the regularized resolvent transform

Geoffrey S. Armstrong,[a] Nikolaus M. Loening,[b,1] Joseph E. Curtis,[a] A.J. Shaka,[a] and Vladimir A. Mandelshtam[a,*]

[a] *Chemistry Department, University of California, Irvine, CA 92697-2025, USA*
[b] *Chemistry Department, University of Cambridge, Lensfield Road, Cambridge CB2 1EW, UK*

Received 13 December 2002; revised 28 March 2003

Abstract

A new method for processing diffusion ordered spectroscopy (DOSY) data is presented. This method, the regularized resolvent transform (iRRT—the i denoting the adaptation of the method to evaluate the inverse Laplace transform), is better than conventional processing techniques for generating 2D DOSY spectra using data that has poor chemical shift resolution. From the same data, it is possible to use the iRRT to generate 1D subspectra corresponding to different components of the sample mixture; these subspectra compare favorably to 1D spectra of the pure substances. Both the 2D spectra and the 1D subspectra offer a vast improvement over results generated using a conventional processing technique (non-linear least-squares fitting). Consequently, we present the iRRT as a stable and reliable tool for solving the inverse Laplace transform problem present in experiments such as DOSY.

Keywords: Spectral estimation; Diffusion ordered spectroscopy; Inverse Laplace transform; Regularized resolvent transform; Filter diagonalization method

1. Introduction

The goal of diffusion ordered spectroscopy (DOSY) [1–3] is to correlate chemical shifts with molecular diffusion coefficients. By doing so, it is possible to assign different peaks in the NMR spectrum to different components of the sample mixture provided that the diffusion coefficients of the components differ. This is useful for analyzing complicated samples, such as biological fluids, where assigning the NMR spectrum might otherwise be difficult. In addition, as the diffusion coefficient of each peak is apparent in a DOSY spectrum, it is possible to use the technique for monitoring processes that affect the diffusion coefficient. For example, such measurements can be used to observe the binding of a drug candidate in a mixture of test compounds to a target molecule [4,5].

In most cases, DOSY involves the acquisition of a 2D dataset in which the directly detected (acquisition) dimension contains the usual NMR free induction decay (FID) and the indirect dimension reflects the variation of this signal due to diffusion. Experimentally, this is realized by acquiring a series of 1D NMR experiments with different amounts of diffusion weighting. After transforming the acquisition dimension, it is possible to extract the diffusion coefficients for each peak in the direct dimension by fitting the variation of the signal in the indirect dimension. From this information it is then possible to generate a DOSY spectrum, which is a 2D plot in which one axis corresponds to the acquisition dimension of the NMR experiment and the other axis corresponds to the apparent diffusion coefficient.

Despite the usefulness of the DOSY technique [4–6], its application has been curtailed by the difficulty of extracting the diffusion coefficients from the data. This is because molecular diffusion only results in a decay of the NMR signal; there are no frequency components in the diffusion dimension of the NMR experiment. Consequently, if the Fourier transform were used to process the diffusion dimension, the resulting spectrum would

* Corresponding author. Fax: 1-949-824-8571.
E-mail address: mandelsh@uci.edu (V.A. Mandelshtam).
[1] Present address: MIT/Harvard Center for Magnetic Resonance, 150 Albany St., Cambridge, MA 02139, USA.

1090-7807/03/$ - see front matter © 2003 Elsevier Science (USA). All rights reserved.
doi:10.1016/S1090-7807(03)00126-5

contain in the indirect dimension peaks centered at zero frequency that differ only in their linewidths. Although the diffusion coefficients could be extracted by fitting the lineshapes in the transformed diffusion dimension, it is better to fit the decay curves directly. With the correct choice for the values of the diffusion weighting gradients, the signal in the indirect dimension can be described by a sum of exponential decays, so for regions of the data where the peaks are well-resolved in the acquisition dimension the analysis of the data is straightforward. In these regions, the diffusion coefficient for each peak can be determined by fitting the decay in the indirect dimension to a monoexponential function using non-linear least-squares.

For parts of the spectrum where the peaks are not well-resolved, the decay curve is multiexponential and, consequently, should be analyzed using more sophisticated techniques. Fitting multiexponential curves is challenging because fundamentally it is an ill-posed problem; for a finite dataset there are multiple solutions all of which fit the data equally well [7]. The addition of noise and/or a baseline offset to the decay curve only exacerbates the problem and, as a consequence, there is a limit to the number of components that can be resolved. In NMR, where the signal-to-noise ratio rarely exceeds 10^3 and the values of possible diffusion coefficients range over several orders of magnitude, one should not expect to be able to resolve more than three diffusion coefficients in realistic situations. Even with a few components in a decay curve, finding the "best" solution is still a challenging problem.

A number of techniques have been developed or implemented to analyze multiexponential decay curves, including non-linear least-squares [8], DISCRETE [1,9], SPLMOD [2,10], DECRA [11], CORE [12], CONTIN [2], and MaxEnt [13]. All of these techniques have their own strengths and weaknesses and, as a consequence, no single technique is the best for all situations. Depending on the technique in question, weaknesses include such things as numerical instability, broad linewidths in the diffusion dimension, spurious artifact peaks, susceptibility to falling into local minima, computational inefficiency, the need to set a threshold level, and/or a requirement for a priori knowledge about the system (such as the number of components).

In this paper, we present a new technique for generating DOSY spectra. We believe that this technique is more generally applicable than the previous techniques, especially for the case of mildly overlapping resonances. This technique, the regularized resolvent transform adapted to solve the inverse Laplace transform (iRRT) is based on the regularized resolvent transform (RRT) [14] which is, in turn, an extension of the filter diagonalization method (FDM) [15–17]. These methods have been used successfully to process multidimensional NMR spectra [18–23] and have many similarities even though the FDM was originally designed to solve the *harmonic inversion problem*, while the RRT was designed to solve the *spectral estimation problem*. As will be seen, the main advantage of the FDM and the RRT is that they are true multidimensional methods. That is, they process the entire multidimensional dataset *at once* rather than processing each dimension independently of the others. In addition, they are relatively computationally inexpensive compared to many other methods, especially those based on non-linear optimization.

In principle both the FDM and the RRT can be used for analyzing DOSY data. However, as the problem of analyzing multiexponential data such as that produced in DOSY experiments is very ill-posed, the regularization aspect of these techniques is crucial [24,25]. In the FDM, one has to regularize an ill-conditioned generalized eigenvalue problem, while in the RRT, it is necessary to regularize an ill-conditioned linear system. It turns out that regularization of the former is very tricky, while regularization of linear systems is straightforward and well understood. Consequently, we have based our method for processing DOSY data on the RRT.

2. Theory

2.1. Formulation of the spectral inversion problem

Although the variation of the signal intensity in the diffusion dimension of the DOSY experiment is Gaussian in nature, it is possible to make the diffusion decay appear exponential by incrementing the gradient in a non-linear manner (as will be explained later in this paper). Therefore, we can describe the NMR data generated in a DOSY experiment as a 2D array $c(n,m)$ composed of a finite number (K) of components that oscillate along the acquisition time dimension (n) and decay exponentially in the diffusion dimension (m):

$$c(n,m) = \sum_{k=1}^{K} d_k u_k^n \lambda_k^m. \tag{1}$$

This model treats noise implicitly so, in practice, K will be larger than the number of real components. The dimensions of the array run from $n = 0,\ldots,N-1$ and $m = 0,\ldots,M-1$; d_k are complex amplitudes that include the phase information. In this representation, the terms

$$u_k = \mathrm{e}^{-\mathrm{i}\tau\omega_k} \quad \text{and} \quad \lambda_k = \mathrm{e}^{-\beta^2\Delta'\alpha_k}$$

contain the parameters for the acquisition dimension and the diffusion dimension, respectively. For the dimensions, τ is the sampling time step (i.e., dwell time) during acquisition, and Δ' is the diffusion delay time corrected for the gradient shape as described later in this paper. Each *complex* frequency, ω_k, contains both a real

part corresponding to the position of a resonance in the spectrum and an imaginary part corresponding to the linewidth of that resonance. In the diffusion dimension, α_k corresponds to the diffusion coefficients and β is a fitting parameter that will be described in the next section. Except for polydisperse samples, there will only be a few different values of α_k and, for all physical cases, these values will consist only of real numbers. However, introducing any numerical constraints on α_k can be problematic and therefore is not done here.

The 2D parameter estimation problem described by Eq. (1) is appealing but is not used here explicitly. Instead, the FDM assumption is made to derive a more convenient working expression [18]:

$$c(n,m) = \Phi^{\mathrm{T}} U^n \Lambda^m \Phi, \tag{2}$$

where Φ is a $K \times 1$ column vector and U and Λ are commuting $K \times K$ complex symmetric matrices, which by definition have the properties

$$U\Lambda = \Lambda U, \quad U^{\mathrm{T}} = U, \quad \Lambda^{\mathrm{T}} = \Lambda.$$

It can be shown by resorting to the spectral representations of U and Λ that Eqs. (1) and (2) are equivalent models for the data [18].

Our objective is to generate an estimate of the 2D spectrum as a function of two real parameters (the proton chemical shift ω and the diffusion coefficient α). If we know d_k, u_k, and λ_k, then we can generate the DOSY spectrum according to the spectral representation

$$I(\omega,\alpha) = \sum_k d_k \frac{1}{(1-u_k/u)} \frac{1}{(1-\lambda_k/\lambda)}, \tag{3}$$

where

$$u = \mathrm{e}^{-\mathrm{i}\tau\omega} \quad \text{and} \quad \lambda = \mathrm{e}^{-\beta^2 \Delta' \alpha}.$$

Note that due to Eq. (1) the double sum

$$I(\omega,\alpha) = \sum_{n=0}^{\infty} \sum_{m=0}^{\infty} c(n,m) u^{-n} \lambda^{-m} \tag{4}$$

is a formal Taylor expansion of $I(\omega,\alpha)$. The summation over n is the usual discrete Fourier sum which is numerically well-behaved. The summation over m, corresponding to a formally divergent series, arises from the inverse Laplace transform. Therefore, this expression cannot be used directly, even in a truncated form.

In practice, we want to avoid having to find explicit solutions for the parameters d_k, u_k, and λ_k. To cast the problem of generating the spectrum into a form where we do not have to solve for d_k, u_k, and λ_k, we can utilize the equivalence of the forms Eqs. (1) and (2) and the form of the spectrum (Eq. (3)) to obtain the resolvent formula [14]

$$I(\omega,\alpha) = \Phi^{\mathrm{T}} \frac{1}{(1-U/u)} \frac{1}{(1-\Lambda/\lambda)} \Phi. \tag{5}$$

Note that, although Eq. (3) is the most natural and simple equation for generating the spectrum, it does not result in the most useful spectral representation as it does not lead to double-absorption lineshapes. Instead, we use the representation

$$A(\omega,\alpha) = \left| \sum_k d_k \frac{1}{(1-u_k/u)^2} \frac{1}{(1-\lambda_k/\lambda)^2} \right| \tag{6}$$

which produces *pseudo-absorption* lineshapes [14]. The only drawback of this representation is that it distorts the peak amplitudes; that is, it scales each peak by a factor equal to the inverse of its linewidth. As a result, sharp peaks are overemphasized relative to broad ones. In terms of the resolvents, Eq. (6) can be written as

$$A(\omega,\alpha) = \left| \Phi^{\mathrm{T}} \frac{1}{(1-U/u)^2} \frac{1}{(1-\Lambda/\lambda)^2} \Phi \right|. \tag{7}$$

2.2. Local spectral analysis using a Fourier basis

Although both Eqs. (5) and (7) are in principle well-behaved, neither can be used directly for spectral estimation as the matrices U and Λ and the vector Φ are not defined. Fortunately, the corresponding resolvent matrix elements can be represented in terms of the available data by choosing a suitable basis. The simplest choice is given by

$$\Phi_{n,m} = U^n \Lambda^m \Phi,$$

where the dimensions run from $n = 0, \ldots, \tilde{N} - 1$ and $m = 0, \ldots, \tilde{M} - 1$, and, assuming that both N and M are even integers, we have defined

$$\tilde{N} = \frac{N}{2} \quad \text{and} \quad \tilde{M} = \frac{M}{2}$$

(rigorously speaking this basis is overdetermined if $\tilde{N}\tilde{M} > K$). Evaluated in this basis the expressions in Eqs. (5) and (7) can be written solely in terms of the available data $c(n,m)$. However, this would require the solution of a linear system with $\tilde{N} \times \tilde{M}$ equations to generate the spectrum. A more appropriate choice corresponds to a small Fourier basis

$$\Psi_j = \sum_{n=0}^{\tilde{N}-1} \sum_{m=0}^{\tilde{M}-1} \left(\frac{U}{z_j} \right)^n \Lambda^m \Phi \quad (j = 1, \ldots, K_{\mathrm{win}}) \tag{8}$$

with a set of values on the unit circle $z_j = \mathrm{e}^{-\mathrm{i}\tau\varphi_j}$. Such a basis effectively represents only important contributions to the resolvent $(1-U/u)^{-1}$ if $z_j \sim u$ (or $\varphi_j \sim \omega$), and to the resolvent $(1-\Lambda/\lambda)^{-1}$ if λ is real. Note that, unlike the conventional case of a 2D Fourier spectral analysis where each dimension is treated on the same footing, here the signal does not oscillate along the diffusion dimension. Consequently, the corresponding Fourier filter is much simpler and is designed to represent only the zero frequency contributions. A further simplification exists

if the set of values $z_j \equiv e^{-i\tau\varphi_j}$ are chosen as K_{win} consecutive roots of unity of the $\tilde{N}$th order [26]

$$z_j^{\tilde{N}} = 1.$$

This corresponds to choosing an equidistant set of real numbers $\varphi_j = 2(j_0 + j)\pi/\tilde{N}\tau$, where $j = 1, \ldots, K_{\text{win}}$ in some a priori specified frequency window.

The whole frequency range of interest is then split into small overlapping windows of equal size (see, e.g. [27]). The spectra in each window are computed and then summed with an appropriate weighting to account for the overlap. Note that with this construction the rank of the original signal space K (see Eq. (1)) is not a parameter of the method. It may seem that the method will now depend on our choice of K_{win}, which determines the size of the local Fourier basis. However, the results are generally insensitive to K_{win} as long as it is sufficiently large. In practice, we find that $K_{\text{win}} = 30$ is usually "sufficiently large" and, at the same time, does not result in overly expensive computations.

2.3. iRRT: working expressions

Numerical expressions to evaluate the spectra in a window basis described by Eq. (8) are given by (see [17] for a derivation of the matrix elements)

$$I(\omega, \alpha) = \mathbf{C}^{\mathrm{T}}\mathbf{R}_1^{-1}\mathbf{U}_0\mathbf{R}_2^{-1}\mathbf{C}, \tag{9}$$

$$A(\omega, \alpha) = \left|\mathbf{C}^{\mathrm{T}}\mathbf{R}_1^{-1}\mathbf{U}_0\mathbf{R}_1^{-1}\mathbf{U}_0\mathbf{R}_2^{-1}\mathbf{U}_0\mathbf{R}_2^{-1}\mathbf{C}\right|. \tag{10}$$

Here the elements of the column vector $\mathbf{C}$ are

$$[\mathbf{C}]_j = \sum_{n=0}^{\tilde{N}-1}\sum_{m=0}^{\tilde{M}-1}\left(\frac{1}{z_j}\right)^n c(n, m)$$

and the $K_{\text{win}} \times K_{\text{win}}$ matrix pencils are defined as

$$\mathbf{R}_1 = \mathbf{U}_0 - \frac{1}{u}\mathbf{U}_1 \quad \text{and} \quad \mathbf{R}_2 = \mathbf{U}_0 - \frac{1}{\lambda}\mathbf{U}_2.$$

The elements for the matrices $\mathbf{U}_p$ $(p = 0, 1, 2)$ are computed using

$$[\mathbf{U}_p]_{jj'} = \begin{cases} \dfrac{z_{j'}x_p(z_j) - z_j x_p(z_{j'})}{z_{j'} - z_j} & \text{if } j \neq j', \\ y_p(z_j) & \text{otherwise,} \end{cases} \tag{11}$$

where

$$x_p(z) = \sum_{n=0}^{\tilde{N}-1} z^{-n}\left(a_p(n) - a_p\left(n + \tilde{N}\right)\right),$$

$$y_p(z) = \sum_{n=0}^{N-2} z^{-n}a_p(n)\left(\tilde{N} - \left|\tilde{N} - n - 1\right|\right)$$

and the three arrays $a_p(n)$ are given by

$$a_p(n) = \sum_{m=0}^{M-2} c(n + n_p, m + m_p)\left(\tilde{M} - \left|\tilde{M} - m - 1\right|\right)$$

with $(n_0, m_0) = (0, 0)$, $(n_1, m_1) = (1, 0)$, and $(n_2, m_2) = (0, 1)$. Even though the points $c(N, m)$ are formally included in the summation for $x_1(z)$, evaluation of the $\mathbf{U}_p$ matrices only requires the knowledge of $c(n, m)$ for $n = 0, \ldots, N - 1 = 2\tilde{N} - 1$ and $m = 0, \ldots, M - 1 = 2\tilde{M} - 1$. The final result for $\mathbf{U}_1$ does not actually depend on $c(N, m)$ as the corresponding contributions in Eq. (11) cancel.

Note that $\mathbf{R}_1$ is a function of the proton frequency ω and $\mathbf{R}_2$ is a function of the diffusion coefficient α. Consequently, $\mathbf{R}_1$ must be inverted at each value of ω and $\mathbf{R}_2$ at each value of α where the spectrum $A(\omega, \alpha)$ is desired. Fortunately, when the Fourier basis is used the matrices are small ($K_{\text{win}} \leqslant 50$), so the computational time is not generally a concern. Instead, the primary issue is the regularization of $\mathbf{R}_1$ and $\mathbf{R}_2$.

Eqs. (9) and (10) are new and constitute one of the main results of this paper. Although they look very similar to those derived for 2D Fourier spectral estimation using the RRT [14], one way in which they differ is that, here, the argument α formally corresponds to the imaginary frequency ($\lambda = e^{-\beta^2\Delta'\alpha}$ is real and not on the unit circle). Another difference is in the way the Fourier basis is set up (Eq. (8)). To emphasize these differences we call the present method the iRRT.

The iRRT performs 2D spectral estimation by evaluating a direct transformation of the original data, and thereby avoids any need to fit the data by non-linear least-squares. Of course, this does not mean that numerical evaluation of Eqs. (9) and (10) are always straightforward: no matter how good the method is, the original inverse Laplace transform problem is ill-posed and therefore the problems associated with instability of the solution cannot be avoided. The instability of the solution is associated with the ill-conditioned nature of the matrices to be inverted ($\mathbf{R}_1$ and $\mathbf{R}_2$) and, despite the very special choice of the Fourier basis in the previous section, the matrices $\mathbf{R}_1$ and $\mathbf{R}_2$ still remain ill-conditioned. However, we have discovered that it is possible to reduce the instabilities in the iRRT spectra by using a two-step regularization scheme.

2.4. Two-step regularization

In principle, the regularization of $\mathbf{R}_1$ and $\mathbf{R}_2$ could be achieved using Tikhonov regularization [14,24], which is significantly faster than, e.g., singular value decomposition (SVD) [8]. The problem with Tikhonov regularization is that the whole procedure must be repeated for each value of the regularization parameter, which is usually unknown in advance. In the case of SVD based regularization, the most computationally intensive part (the SVD) needs to be applied only once, so the generation of spectra for different values of the regularization parameter requires minimal extra work. For this reason, we have found it advantageous to use a scheme based on SVD. In SVD, the matrix that we wish to invert ($\mathbf{R}$) is decomposed according to:

$$\mathbf{R} = \mathbf{V}\boldsymbol{\Sigma}\mathbf{W}^{\dagger},$$

where $\mathbf{V}$ and $\mathbf{W}$ are unitary matrices, and $\boldsymbol{\Sigma} = \mathrm{diag}(\sigma_i)$ is a diagonal matrix in which σ_i are real positive values. After performing SVD, the inverse ($\mathbf{R}^{-1}$) can be readily calculated. However, since the elements σ_i can be small or even zero, their reciprocals may be very large leading to unphysical results.

An effective regularization replaces the true inverse

$$\mathbf{R}^{-1} = \mathbf{W}\boldsymbol{\Sigma}^{-1}\mathbf{V}^{\dagger} \tag{12}$$

by a pseudo-inverse. For example, this can be accomplished using

$$\mathbf{R}_q^{-1} = \mathbf{W}\boldsymbol{\Sigma}_q^{-1}\mathbf{V}^{\dagger}, \tag{13}$$

where

$$\boldsymbol{\Sigma}_q = \mathrm{diag}\left(\frac{\sigma_i^2 + q}{\sigma_i}\right)$$

and q is a regularization parameter that is small and positive, but generally unknown. To determine the optimal value of q, several spectra $A_q(\omega,\alpha)$ using different values of q are generated and analyzed to identify which value of q retains what are believed to be true peaks, but removes most of the artifacts associated with the ill-conditioned nature of the problem. Very often there may be no "optimal" value of q. For instance, an increase of q may remove the correct structure together with the artifacts, so a compromise must be found. For the present problem, the use of SVD (as well as Tikhonov) regularization on its own requires too much fiddling with q to reach a reasonable compromise. Even more importantly, one has little control on how individual peaks are being "regularized." For instance, some peaks may be arbitrarily narrow in the diffusion dimension (in fact, the peak "width" in α is an ambiguous quantity) leading to spectra that are difficult to contour and interpret.

Much better results are obtained by implementing a two-step regularization. In the first step SVD regularization is used with a smaller value of q than is usual. This applies a mild regularization that does not remove the correct structures but may leave some artifacts. The second step corresponds to a frequency-correlated regularization, via a Lorentz–Gauss convolution

$$A_{q\sigma}(\omega,\alpha) = \int \mathrm{d}\omega'\mathrm{d}\alpha' A_q(\omega',\alpha') \exp\left[-\left(\frac{\omega-\omega'}{2\sigma_\omega}\right)^2 - \left(\frac{\alpha-\alpha'}{2\sigma_\alpha}\right)^2\right], \tag{14}$$

where σ_ω and σ_α are adjustable smoothing parameters. This has the effect of smoothing the spectrum and attenuating the remaining artifacts. Also, as the smoothing is applied *after* the spectrum is generated, it does not decrease the numerical efficiency of the method. Because we can still tolerate some artifacts left from the SVD regularization, it is not important that the parameter q is heavily optimized. Therefore, it is possible to set q to some small value and thus mostly eliminate the dependence of the method on the exact value of q.

Since the actual value of q must be a function of the signal norm

$$\|c\| = NM\sum_{n=0}^{N-1}\sum_{m=0}^{M-1}|c(n,m)|,$$

it is more convenient to use the scaled parameter

$$\tilde{q} = q\frac{1}{\|c\|} \tag{15}$$

which is not sensitive to either scaling the signal or changing its size. The typical range for $\tilde{q}$ is between 0.1 and 0.01. Although smoothing along ω may be needed, here it was not necessary. This twofold method of regularization may seem redundant and somewhat inefficient because of the need to generate the spectrum, $A_q(\omega,\alpha)$, with a sufficiently fine grid of values in order to evaluate accurately the integral in Eq. (14). However, we believe this to be the best method at this time. Although it may be possible to incorporate both regularization steps into a single regularization, so far, we have not found a successful implementation of such a method.

3. Experimental setup

To test the utility of the iRRT for generating DOSY spectra, we choose a challenging sample system consisting of geraniol (20 μl), camphene (30 mg), and quinine (27 mg) in 500 μl of deuteromethanol. This sample was chosen because, due to spectral overlap, the aliphatic region of the spectrum serves as a good test of how well a method can resolve peaks based on their diffusion coefficients. In addition, the diffusion coefficients are relatively close together, which makes separating the peaks especially challenging. This system was used by Barjat et al. [28] as a test sample for their 3D DOSY-HMQC experiment; by using the iRRT, it is possible to effectively resolve most peaks using a 2D experiment, obviating the need to add a carbon dimension to the experiment.

A modified DSTE [29] pulse sequence was used (Fig. 1) to ensure that sample convection would not interfere with the results. This is important as sample convection would, if present, add a non-exponential component to the signal decay and result in spurious peaks in the DOSY spectrum. In addition, a z-filter was added immediately before signal acquisition by introducing a period with simultaneous spin-lock and gradient pulses [30]. This removes small antiphase coherences that develop for coupled spins during the final refocusing gradient pulse.

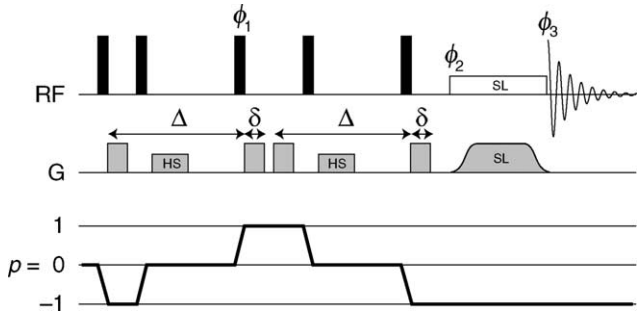

Fig. 1. The DSTE pulse sequence used for the DOSY experiments. From top to bottom, the lines indicate the timing of the radiofrequency pulses (RF), the gradient pulses (G), and the coherence order (p). The diffusion weighting gradient pulses have length δ; Δ indicates the diffusion delay. Homospoil gradients are labeled "HS" and the spin-lock pulse is labeled "SL." All pulses have phase x except for $\phi_1 = (x, -x)$, $\phi_2 = (y)$, and $\phi_3 = (x, -x)$.

The DOSY experiments were performed on a 500 MHz (^{1}H) Bruker Avance DRX500 spectrometer. For all experiments, the sample temperature was maintained at 300 ($\pm$0.1) K. The gradients were shaped to a half sine-bell, so the diffusion delay corrected for the gradient shape (Δ') is

$$\Delta' = \Delta - \frac{1}{4}\delta,$$

where Δ is the length of time from the start of the first diffusion-weighting gradient to the start of the second diffusion-weighting (refocusing) gradient, and δ is the length of the gradient pulse (see Fig. 1). We define the gradient area, g, as

$$g = \frac{2}{\pi}\gamma G\delta.$$

This quantity depends on the magnetogyric ratio γ, the physical gradient strength G, the gradient pulse length, and includes a factor of $2/\pi$ to account for the shape of the gradient. For our experiment, the diffusion delay time, Δ, was 52 ms and the gradient pulse length, δ, was 2 ms. The dwell time in the directly detected dimension was 224 μs. The peak strength of the diffusion weighting gradients were 14.23, 20.12, 24.64, 28.45, 31.81, 34.85, 37.64, and 40.24 G cm^{-1}; these values were chosen so that the diffusion dependent decay in the indirect dimension appears to be exponential, as described in the next paragraph. While 8192 points were collected in the direct dimension, only 8 points were used in the diffusion dimension.

As mentioned previously, the way the data is sampled in the indirect dimension is crucial to the processing. In order to satisfy the assumptions of the method (Eq. (1)), the signal must behave as a sum of complex or real exponentials in all dimensions. For DOSY, the signal in the diffusion dimension decays as

$$\frac{S}{S_0} = \mathrm{e}^{-D\Delta' g^2} \tag{16}$$

which is Gaussian if g is sampled linearly. However, it is possible to vary g non-linearly to enforce the exponential behavior that is required. In our case, g was chosen according to $g = \beta\sqrt{m}$, where β is adjusted to give an appropriate amount of diffusion weighting. This method of sampling results in the required form for the signal.

4. Numerical results

The iRRT spectra presented here were processed using Eqs. (10), (13), and (14) with $N = 6000$, $M = 8$, $K_{\mathrm{win}} = 30$, $\tilde{q} = 0.1$, $\sigma_\omega = 0$, and $\sigma_\alpha = 1.6 \times 10^{-7}$. Note that the iRRT spectrum exhibits high resolution in both dimensions even though only 8 points are used in the diffusion dimension. This is because the iRRT is a multidimensional method: the resolution in both dimensions depends on the *total* number of data points (6000×8).

For comparison purposes we also processed the DOSY data using a more conventional technique. This involves applying the Fourier transform to the acquisition dimension followed by performing an exponential fit for each frequency point. In this case, we used the most straightforward algorithm; the decay curves were fit to a monoexponential decay using the Levenberg–Marquardt non-linear least-squares algorithm [8]. The starting parameters for the non-linear fitting were determined by initially fitting the data using linear-least-squares; this ensured that the fit converged to a realistic minimum.

The diffusion coefficient, α_ω, and the standard deviation, ξ_ω, that result from the fitting routine are then used to construct the spectrum as follows:

$$I(\omega, \alpha) = \frac{A_0(\omega)}{\sqrt{2\pi\xi_\omega^2}}\mathrm{e}^{-((\alpha-\alpha_\omega)^2/2\xi_\omega^2)},$$

where $A_0(\omega)$ is the FT of the first increment of the DOSY experiment. This method results in Gaussian lineshapes in the diffusion dimension centered at the diffusion coefficient and with a linewidth equal to the uncertainty returned by the fitting routine. This is the standard method for generating DOSY spectra [1–3].

Although fitting the data to a monoexponential function does not yield as much information as is available from other methods, it has the advantage that it "fails" in a known way and the result of such a failure can be easily identified. The routine fails when there are multiple components in the decay curve as the routine only has enough parameters to model a single component. The result of such a failure is usually a peak that spreads diagonally across the spectrum; this effect is often seen in the tails of peaks. More sophisticated methods may yield "cross peaks" which can be mistaken for true peaks and are much more difficult to spot.

In Fig. 2, we present the 2D DOSY spectra of the mixture. In well-separated regions of the spectrum the

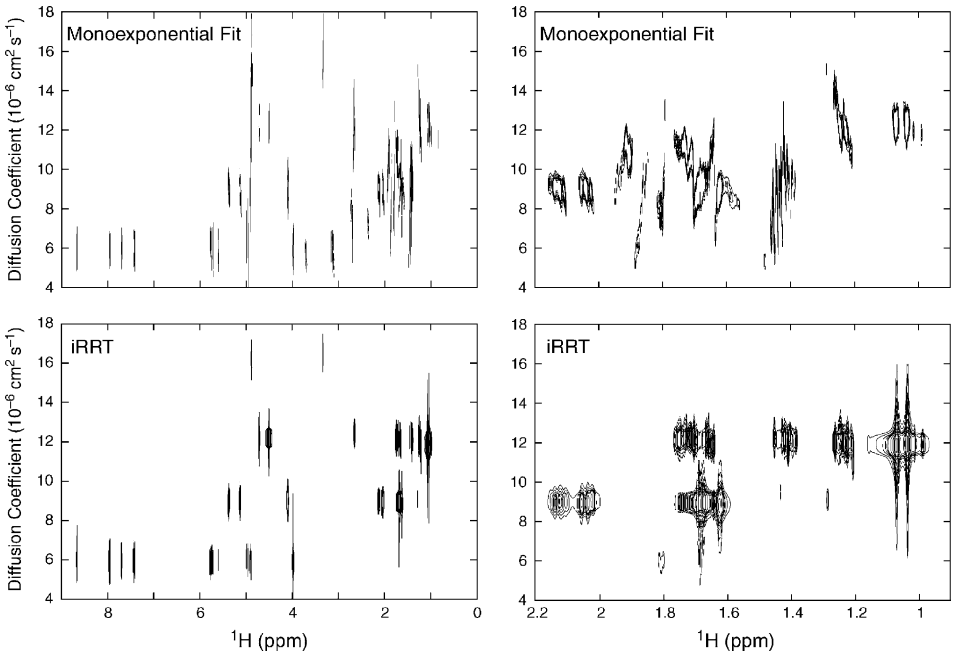

Fig. 2. Comparison of DOSY spectra constructed using non-linear least-squares fitting to a monoexponential decay and using the iRRT. The spectra on the left show the full spectrum; those on the right show an expanded view of the aliphatic region. Both methods are effective in the regions of the spectrum where the peaks are well-resolved in the acquisition dimension. However, in the aliphatic region of the spectrum the peaks are not well-resolved in the acquisition dimension. In this region, the expected behavior of the monoexponential fitting routine is seen; overlapped peaks appear at a point in the diffusion dimension that is the weighted average of the individual components of the decay. In contrast, the iRRT produces uniform results across the entire spectral width and shows better resolution for the aliphatic region. Note that one severely overlapped peak is too weak to show up in the iRRT spectrum at this contour level.

monoexponential fit is adequate, but in the crowded aliphatic region, the results reflect weighted averages of overlapped peaks and make it difficult or impossible to assign peaks to a particular component. In the iRRT spectrum, however, peaks in both the aliphatic region and the remaining parts of the spectrum are fairly well resolved. For all parts of the iRRT spectrum and well-resolved parts of the monoexponential fit spectrum, the diffusion coefficients for the three components are apparent: for camphene $D = (12.4 \pm 0.5) \times 10^{-6}\,\mathrm{cm^2\,s^{-1}}$, for geraniol $D = (9.1 \pm 0.5) \times 10^{-6}\,\mathrm{cm^2\,s^{-1}}$, and for quinine $D = (6.1 \pm 0.3) \times 10^{-6}\,\mathrm{cm^2\,s^{-1}}$.

While the 2D spectrum is useful for noting the spectral separation for different species and for obtaining the diffusion coefficients, the more useful feature of DOSY is the ability to make structural assignments of individual components in a mixture. This can be done by viewing 1D cross-sections of the 2D spectrum. Since there is some error in the diffusion coefficient of individual peaks, these subspectra should be generated by integrating over a small range in the diffusion dimension. This results in a more representative 1D spectrum of the component.

Identical integration ranges have been used to obtain subspectra of the individual components from both the non-linear least-squares DOSY spectrum and the iRRT DOSY spectrum. The resulting subspectra corresponding to camphene, geraniol, and quinine are presented in Fig. 3 along with spectra of the pure substance (solvated in deuteromethanol) generated using the FT and the RRT. For the 1D RRT results, the spectra were generated using the pseudo-absorption mode (which distorts the amplitudes) to make them more consistent with the 1D subspectra generated from the 2D iRRT DOSY spectrum. In all the figures, solvent peaks due to the residual protonated solvent and HOD are labeled with asterisks (*).

For the camphene subspectra (Fig. 3), the iRRT is able to reproduce all but one of the resonances present in the pure substance without introducing any incorrect peaks. The monoexponential fit is also able to produce most of the resonances, but in the crowded region several of the resonances are missing. In addition, one of the solvent peaks is not completely removed in the non-linear least-squares subspectrum. For geraniol (Fig. 3), both methods reproduce all of the resonances in the pure spectrum. However, whereas the iRRT slice contains very few incorrect peaks, the monoexponential fit contains numerous artifacts from the tails of the Gaussian quinine, camphene, and solvent peaks in the diffusion dimension. Finally, the quinine subspectra (Fig. 3) reveal the limitations of both methods. In the aliphatic region, the intensity for both methods is severely reduced due to the fact that the intensity is spread across two other much stronger components (the concentrations of camphene and geraniol in the sample are

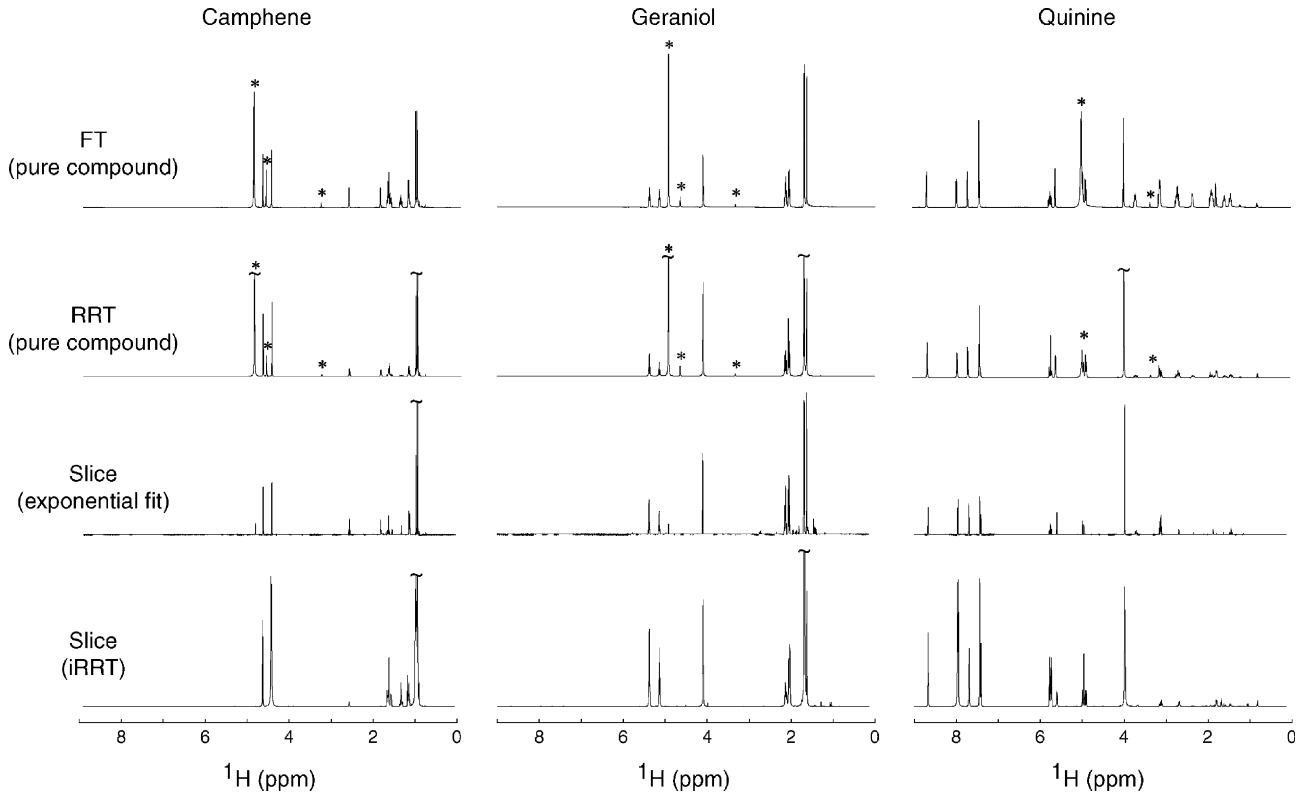

Fig. 3. 1D spectra and DOSY subspectra for the three components of the mixture (camphene, geraniol, and quinine). Solvent peaks are indicated with asterisks (*). For the camphene subspectra, all but one peak is reproduced by the iRRT, and the structure in the aliphatic region is much better preserved than in the subspectrum from the monoexponential fit. Also, note that one of the solvent peaks is still present in the spectrum from the monoexponential fit. For geraniol, both methods effectively resolve all the peaks, but the peak structure is much more prominent in the iRRT subspectrum. In addition, peaks from the solvent, camphene, and quinine are not completely removed in the subspectrum based on the monoexponential fit. Finally, for quinine, subspectra generated using both methods suffer from reduced intensity in the aliphatic region. However, for the subspectrum generated from the iRRT spectrum, most of the resonances are still present. Note that in the case of quinine, the subspectrum based on the iRRT is able to reveal structure around 5 ppm that was completely obscured by solvent; this structure does not appear in the spectrum based on using a monoexponential fit.

higher than the concentration of quinine). This suggests that for samples with overlapping resonances, and a large range of concentrations, the iRRT may still be limited in the results that it can provide. Despite this, almost all of the resonances are reproduced by the iRRT. In other regions of the spectrum, the iRRT reproduces the structure exactly, while the monoexponential fit is, as would be expected, unable to reproduce resonances that overlap with the much larger solvent peak. This shows that the iRRT is able to reveal resonances that are not even visible in the pure spectrum.

Fig. 4 illustrates how, in the aliphatic region of the spectrum, both methods suffer limitations. In the case of geraniol, both methods produce the correct structure, but the monoexponential fit contains numerous peaks that are not present in the pure spectrum; as mentioned before, these peaks in the diffusion dimension arise from the tails of the Gaussian peak shapes of other components. It should also be noted that both methyl peaks at 1.7 ppm are present in the iRRT spectrum, but are so intense that they are not seen using this scale; this distortion of the intensities is the disadvantage of using the pseudo-absorption representation. This effect is also seen in the case of camphene, where the iRRT does a much better job of reproducing the fine structure in the 1D spectrum, but the intensity of the peak at 1.9 ppm is reduced to such an extent that it is not easily seen with the present scaling.

5. Conclusions

In this paper we showed how the RRT could be adapted to solve a 2D spectral estimation problem corresponding to a Fourier transformation in the acquisition dimension and an inverse Laplace transformation in the indirect dimension. Due to the severely ill-conditioned nature of the problem, a twofold regularization scheme was adopted to obtain the best results. The two steps of the regularization process involved first adjusting the regularization parameter q used in the SVD step, followed by a Lorentz–Gauss convolution to

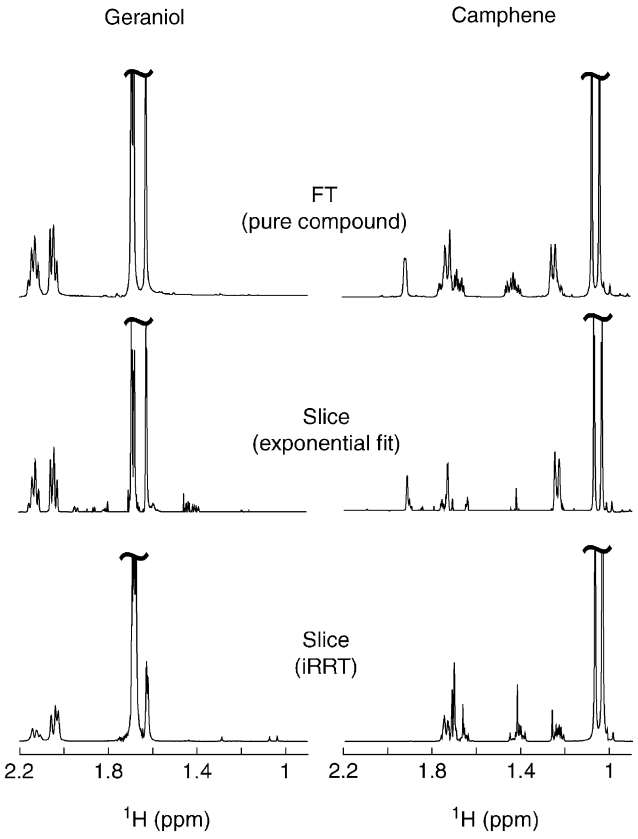

Fig. 4. Expanded aliphatic region of 1D slices for geraniol (left) and camphene (right). For comparison, the FT spectra of the pure compounds are also shown. It can be seen that the spectra generated using the iRRT and monoexponential fitting both suffer from problems in this region. The important point is that, although some of the amplitudes are distorted in the iRRT spectra (as is expected), these spectra, unlike those based on monoexponential fitting, do not contain peaks that are not present in the pure compound.

smooth any remaining artifacts. By applying this method to DOSY, significant improvements can be obtained over monoexponential non-linear least-squares fitting. We were relatively successful in being able to reproduce 1D subspectra corresponding to the pure substances from the 2D iRRT DOSY spectrum of a mixture of a few components. Due to the nature of the iRRT, it is well suited for samples which have a few discrete components that overlap in the chemical shift dimension(s) but is not generally applicable to samples with a large number of overlapping components such as polydisperse samples.

Although the iRRT produces reasonable (and often better) results compared to other methods for processing DOSY spectra, it is still constrained by the limitations of trying to resolve multiple diffusion coefficients from a noisy multiexponential decay curve. This is a problem that is fundamental to 2D DOSY spectroscopy and will not be improved by using other data processing techniques. The way to get around this problem is to add another dimension to the experiment. Although adding dimensions using conventional processing techniques requires large increases in the experiment time, methods based on the FDM/RRT only require modest increases in the experiment time as only a few increments are required in the additional indirect dimensions. In our forthcoming papers, we will show how the present technique can be generalized to such higher dimensional DOSY experiments.

Acknowledgments

We would like to thank Dr. Jianhan Chen for his contributions to writing the original RRT code, and Arnold Neumaier for his helpful discussions. Also, we thank Dr. James Keeler for his insights and discussions. N.M.L. thanks the Winston Churchill Foundation (USA), the Overseas Research Studentship Scheme (UK), and the National Science Foundation Graduate Research Fellowship program (USA) for support. V.A.M. and A.J.S. acknowledge support from the National Science Foundation (USA) under Grants CHE-0108823 and CHE-9900422. V.A.M. would like to thank the Alfred P. Sloan Foundation for supporting him as a research fellow.

References

[1] K.F. Morris, C.S. Johnson Jr., Diffusion-ordered two-dimensional nuclear magnetic resonance spectroscopy, J. Am. Chem. Soc. 114 (1992) 3139–3141.
[2] K.F. Morris, C.S. Johnson Jr., Resolution of discrete and continuous molecular size distributions by means of diffusion-ordered 2D NMR spectroscopy, J. Am. Chem. Soc. 115 (1993) 4291–4299.
[3] C.S. Johnson Jr., Diffusion ordered nuclear magnetic resonance spectroscopy: principles and applications, Prog. Nucl. Magn. Reson. Spectrosc. 34 (1999) 203–256.
[4] M.F. Lin, M.J. Shapiro, J.R. Wareing, Diffusion edited NMR-affinity NMR for direct observation of molecular interactions, J. Am. Chem. Soc. 119 (1997) 5249–5250.
[5] M.F. Lin, M.J. Shapiro, J.R. Wareing, Screening mixtures by affinity NMR, J. Org. Chem. 62 (1997) 8930–8931.
[6] T.L. James, G.G. McDonald, Measurement of the self diffusion coefficient for each component in a complex system using pulsed-gradient Fourier transform NMR, J. Magn. Reson. 11 (1973) 58–61.
[7] A.A. Istratov, O.F. Vyvenko, Exponential analysis in physical phenomena, Rev. Sci. Instrum. 70 (1999) 1233–1257.
[8] W.H. Press, S.A. Teukolsky, W.T. Vetterling, B.P. Flannery, Numerical Recipes in C, second ed., Cambridge University Press, Cambridge, 1992.
[9] S.W. Provencher, An eigenfunction expansion method for the analysis of exponential decay curves, J. Chem. Phys. 64 (1976) 2772–2777.
[10] S.W. Provencher, R.H. Vogel, Regularization techniques for inverse problems in molecular biology, in: P. Deuflhard, E. Hairer (Eds.), Numerical Treatment of Inverse Problems in Differential and Integral Equations, Birkhäuser, Boston, 1983, pp. 304–319.

[11] W. Windig, B. Antalek, Direct exponential curve resolution algorithm (DECRA): a novel application of the generalized rank annihilation method for a single spectral mixture dataset with exponentially decaying contribution profiles, Chemom. Intell. Lab. Syst. 37 (1997) 241–254.
[12] P. Stilbs, K. Paulsen, P.C. Griffiths, Global least-squares analysis of large, correlated spectral datasets: application to component resolved FT-PGSE NMR spectroscopy, J. Phys. Chem. 100 (1996) 8180–8189.
[13] M.A. Delsuc, T.E. Malliavin, Maximum entropy processing of DOSY NMR spectra, Anal. Chem. 70 (1998) 2146–2148.
[14] J. Chen, A.J. Shaka, V.A. Mandelshtam, RRT: the regularized resolvent transform for high resolution spectral estimation, J. Magn. Reson. 147 (2000) 129–137.
[15] M.R. Wall, D. Neuhauser, Extraction, through filter-diagonalization, of general quantum eigenvalues or classical normal mode frequencies from a small number of residues or a short-time segment of a signal. I. Theory and application to a quantum-dynamics model, J. Chem. Phys. 102 (1995) 8011–8022.
[16] V.A. Mandelshtam, H.S. Taylor, Harmonic inversion of time signals and its applications, J. Chem. Phys. 107 (1997) 6756–6769.
[17] V.A. Mandelshtam, FDM: the filter diagonalization method for data processing in NMR experiments, Prog. Nucl. Magn. Reson. Spectrosc. 38 (2001) 159–196.
[18] V.A. Mandelshtam, H.S. Taylor, Multidimensional harmonic inversion by filter-diagonalization, J. Chem. Phys. 108 (1998) 9970–9977.
[19] M.R. Wall, T. Dieckmann, J. Feigon, D. Neuhauser, Two-dimensional filter-diagonalization: spectral inversion of 2D NMR time-correlation signals including degeneracies, Chem. Phys. Lett. 291 (1998) 465–470.
[20] V.A. Mandelshtam, N.D. Taylor, H. Hu, M. Smith, A.J. Shaka, Highly resolved double absorption 2D NMR spectra from complex severely truncated 2D phase modulated signals by filter-diagonalization-averaging method, Chem. Phys. Lett. 305 (1999) 209–216.
[21] V.A. Mandelshtam, The multidimensional filter diagonalization method. I. Theory and numerical implementation, J. Magn. Reson. 144 (2000) 343–356.
[22] A.A. De Angelis, H. Hu, V.A. Mandelshtam, A.J. Shaka, The multidimensional filter diagonalization method. II. Applications to 2D, 3D and 4D NMR experiments, J. Magn. Reson. 144 (2000) 357–366.
[23] J. Chen, V.A. Mandelshtam, A.J. Shaka, Regularization of the filter diagonalization method: FDM2k, J. Magn. Reson. 146 (2000) 363–368.
[24] A. Tikhonov, Solution of incorrectly formulated problems and the regularization method, Soviet Math. Dokl. 4 (1963) 1035–1038; A. Tikhonov, V. Arsenin, Solutions of Ill-posed Problems, Winston and Sons, Washington, 1977.
[25] A. Neumaier, Solving ill-conditioned and singular linear systems: a tutorial on regularization, SIAM Rev. 40 (1998) 636–666.
[26] A. Neumaier, Harmonic inversion problem, preprint, unpublished.
[27] J. Chen, V.A. Mandelshtam, Multiscale filter diagonalization method for spectral analysis of noisy data with nonlocalized features, J. Chem. Phys. 112 (2000) 4429–4437.
[28] H. Barjat, G.A. Morris, A.G. Swanson, A three-dimensional DOSY-HMQC experiment for the high-resolution analysis of complex mixtures, J. Magn. Reson. 131 (1998) 131–138.
[29] A. Jershow, N. Müller, Suppression of convection artifacts in stimulated-echo diffusion experiments. Double-stimulated-echo experiments, J. Magn. Reson. 125 (1997) 372–375.
[30] A.L. Davis, G. Estcourt, J. Keeler, E.D. Laue, J.J. Titman, Improvement of z filters and purging pulses by the use of zero-quantum dephasing in inhomogeneous B_1 or B_0 fields, J. Magn. Reson. A 105 (1993) 167–183.